World Conference on Timber Engineering Oslo 2023

EVALUATION OF MODELS OF FIBRE ORIENTATION IN SAWN TIMBER USING SYNCHRONISED COMPUTED TOMOGRAPHY AND OPTICAL SCANNING DATA

Johannes A. J. Huber[1], Osama Abdeljaber[2], Johan Oja[3], Anders Olsson[4]

ABSTRACT: Optical scanning and X-ray computed tomography (CT) scanning of sawn timber provide a large number of data points, on which data-driven numerical models can be based for simulations. These models require information about the deviations of the fibre orientations in the vicinity of knots. Optical scanning can be used to measure the in-plane fibre orientation on wood surfaces. In CT scans of sawn timber, the fibre orientation around knots can be estimated using a new fibre reconstruction algorithm based on the density gradient. The goal of this paper is to compare and synchronise optical and CT scanning data of sawn timber and then use the combined data set to evaluate fibre orientations derived from both representations. The material comprised sawn timber of Norway spruce, in which alignment holes were drilled. The timber was scanned in an industrial CT scanner and subsequently in an industrial optical scanner where scanning was repeated after successive planing of the sawn timber surface. The results show that a projective mapping in combination with a spline interpolation are required for synchronisation, and that the in-plane fibre orientations calculated from the density gradients are qualitatively similar to the orientations derived from the optical data.

KEYWORDS: Knots, Tracheid effect, CT scanning, Strength grading, Image analysis, Gradient structure tensor

1 INTRODUCTION

Strength-graded sawn timber constitutes the base of most solid timber-based structures or engineered wood products used in these structures. Knowledge about the mechanical properties of the used timber is therefore imperative for design. For individual pieces of sawn timber, the exact values of these properties are, however, unknown and for strength specifically, they are inherently unknowable without destructive tests.

In machine strength grading, *indicating properties* (IPs) of sawn timber are used in regression models to predict the *grade-determining properties* density, stiffness and strength. For timber graded into C classes, stiffness and strength relate respectively to the bending modulus of elasticity (MoE) and the bending modulus of rupture (MoR), according to the European standard EN 408 [1]. Sawn timber is graded into a few strength classes at sawmills, where the properties of each class are governed by the characteristic values of strength and density, respectively, and by the characteristic mean value of the MoE. IPs can be derived from various measurements using different technologies [2], but usually large variations in the mechanical properties of individual pieces of sawn timber remain, with coefficients of variation often exceeding 20%.

Comparatively high prediction accuracy can be achieved by IPs based on measuring the in-plane fibre orientation on sawn timber surfaces by laser scanning utilising the tracheid effect [3]. This technology accounts for both the presence of knots and the resulting fibre deviations around knots on the board surface. Nevertheless, the plethora of data points needs to be condensed to one or a few scalar parameters for IP-based predictions in regression models.

Recently, some sawmills have also adapted X-ray computed tomography (CT), currently used for sorting logs and to optimise log positioning regarding yield before sawing [4]. The supplied density data in the log volume lends itself for an automated detection of the location of the pith and knots by image analysis [5]. The

[1] Johannes A. J. Huber, Luleå University of Technology, Skellefteå, Sweden, johannes.huber@ltu.se

[2] Osama Abdeljaber, Linnaeus University, Växjö, Sweden, osama.abdeljaber@lnu.se

[3] Johan Oja, Luleå University of Technology, Skellefteå, Sweden, johan.oja@ltu.se

[4] Anders Olsson, Linnaeus University, Växjö, Sweden, anders.olsson@lnu.se

https://doi.org/10.52202/069179-0057

abundant 3D data gathered is however currently not used for prior-to-sawing strength evaluations.

Knots, and the deviations of the fibre orientation caused by them, strongly affect the stiffness and strength of sawn timber. The complex patterns of fibre orientations around knots have been investigated using laser scanning in successively planed sections of sawn timber [6], and in greater detail by using micro-CT scanning [7].

Gathering high-resolution data of sawn timber facilitates the use of numerical models, e.g. 3D finite element (FE) models, for predicting the properties of individual boards. These models require information about wood features like the pith location, the size and shape of knots, and the fibre orientations. Apart from measuring the in-plane fibre orientation, optical surface data can be used to find knots and determine the location of the pith [8]. Surface data has been used previously for FE models, e.g. to predict the bending stiffness profile in [9], where the location of the pith was estimated by fitting concentric circles to growth rings, the knots were idealised as cones and the fibre deviations were calculated on the basis of a mathematical model [10].

In a recent study [11], CT data also has been used to create FE models of the exact shape of sawn timber, whereby image analysis methods were used to locate the pith, detect knots, and furthermore reconstruct the 3D fibre orientations around knots in a new way, which accounts for irregular shapes of knots. To refine the methodology in [11], verifications are required for the fibre orientations and the size of the regions around knots in which the fibres are disturbed. In the future, CT-based modelling could also be used for logs, to predict the mechanical properties of individual virtual boards in logs already before sawing.

Data-driven models which incorporate the rich data of measurements on individual logs or individual pieces of sawn timber can yield accurate predictions and can facilitate the production of timber with bespoke mechanical properties instead of being binned into predefined strength classes with high variability. Tracking individual pieces and their properties also opens the possibility of planning their structural use in a construction already at the sawmill, as part of a purpose-based grading process.

The objective of this study is therefore to compare and synchronise the high-resolution data obtained from optical scanning and CT scanning, respectively, of sawn timber. More specifically, the goal is to use the combined data set to evaluate fibre orientations around knots derived from both data sets.

2 MATERIAL & METHODS

2.1 MATERIAL PREPARATION

Norway spruce (*picea abies*) sawn timber from Sweden with dimensions 45 × 145 × 3600 mm^3 was prepared by drilling positioning holes at equally spaced positions, see Figure 1. Starting at a lengthwise distance of 50 mm from each edge, and subsequently spaced 700 mm from the first position, three holes at each wide face and two holes on each short face were drilled. The outer holes on the wide faces and the holes on the short faces were spaced 15 mm from the edges of the sawn timber. The third hole on the wide face was centred between the edge holes. At 1450 mm from each edge, only a single hole in the middle of the wide faces was drilled.

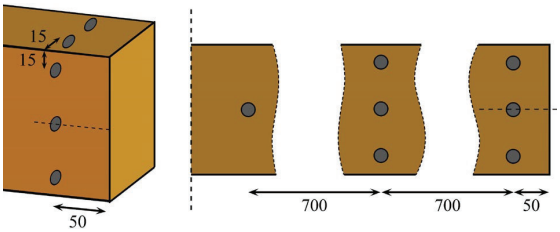

***Figure 1**: Arrangement of the positioning holes*

2.2 DATA ACQUISITION

CT images were acquired of the timber using an industrial CT scanner (Microtec Mito) adapted for research purposes at the facilities of Luleå University of Technology in Skellefteå, Sweden. The sawn timber was wrapped in plastic to contain its moisture content and simply supported at its ends and standing upright, which minimised the bending deflection under its own weight while the scanner moved along the timber, see Figure 2. The reconstructed 3D image stack had a voxel (3D pixel) size of 0.3 × 0.3 × 0.3 mm^3. Each voxel carried a 16-bit grayscale value which represented density in kg/m^3 at the corresponding location.

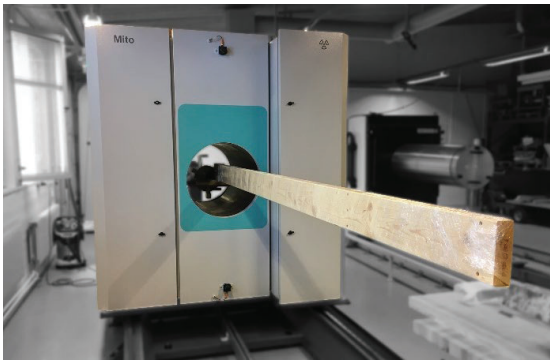

***Figure 2**: CT scanner moving along the sawn timber*

After transport and removal of the plastic wrapping, the sawn timber was scanned using the industrial optical wood scanner Microtec WoodEye (WE) at the facilities of Linnaeus University in Växjö, Sweden. The scanner recorded RGB images of all faces at a pixel size of 0.8 × 0.07 mm^2 (lengthwise × crosswise) and it recorded the in-plane fibre directions using laser tracheid scans at a resolution of 1 × 4.4 mm^2 (lengthwise × crosswise).

To receive a distribution of the in-plane direction in the volume of the boards, the timber was planed successively by a depth of 1 mm at each wide face**,** and after each planing operation, the optical scanning process was repeated, see Figure 3. Nine slices were planed off on each wide face, i.e. 18mm were removed in total.

https://doi.org/10.52202/069179-0057

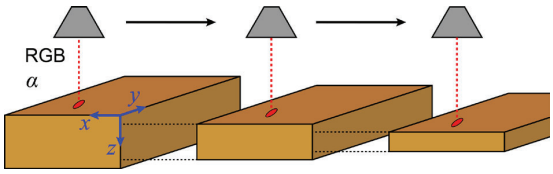

***Figure 3**: Progressively planing and optical scanning*

2.3 CT IMAGE PROCESSING

The CT images represented an equally spaced rectangular grid of density values $\rho(x, y, z)$ in 3D space. The processing of the CT data was primarily performed using code in Julia [12]. For segmenting timber from air, a binary image $B(x, y, z)$ was created by thresholding ρ and filling internal holes.

Since the timber was twisted around its long axis, a misalignment existed between the sawn timber surfaces and the axes of the CT image. To be able to compare flat surfaces in the WE data to corresponding surfaces in the CT images, the latter first needed to be "untwisted". The twist was corrected by rotating and aligning each cross-sectional CT slice to the image axes, see Figure 4. This required estimating the twist angle θ_i of each CT cross-section along a board as well as the translation in both directions (Δx_i and Δz_i) from a fixed reference point. To do so, in each CT cross-section in B the shift in both directions Δx_i and Δz_i from the centroid of the resulting region to the reference point as well as the angle θ_i that the principal axis of the region makes with the horizontal image axis were calculated. These values indicate how much each cross-section should be translated and rotated to straighten the board. The estimates of these values were affected by noise in the CT images, which was partly due to the plastic wrapping around the timber and reconstruction artefacts present in the images. A moving mean filter was therefore applied to denoise the variations of Δx_i, Δz_i, and θ_i before correcting the twist of the board.

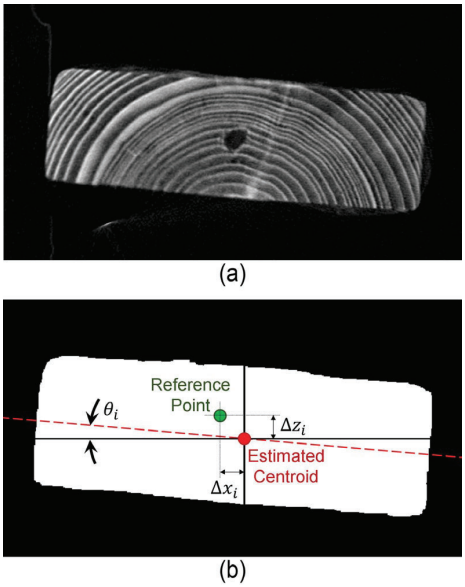

***Figure 4**: Correction of twist in boards; twisted cross-sectional CT image (a), and estimated parameters for untwisting (b)*

To estimate the fibre orientation (*l*-direction) in the untwisted CT image, an adapted version of the method presented in [11] was applied, which is based on finding the smallest gradient in the density field [13]. In a first step, the partial derivatives of the density were calculated by Equation (1).

$$\rho_x = \frac{\partial \rho}{\partial \mathrm{x}} \approx w_{\sigma 1} * (w_{\Delta x} * \rho) \tag{1}$$

where $w_{\Delta x}$ is a convolutional kernel for finite differences [14], $w_{\sigma 1}$ is a Gaussian kernel with a standard deviation of 1 voxel and ρ from here on represents the density of the untwisted CT image. The partial derivatives were equivalently calculated for y and z. In a second step, the *gradient structure tensor* (GST) was constructed, see Equation (2).

$$\mathrm{GST}\big(\rho(x,y,z)\big) = w_{\sigma 2} * \begin{pmatrix} \rho_x^2 & \rho_x\rho_y & \rho_x\rho_z \\ & \rho_y^2 & \rho_y\rho_z \\ \mathrm{sym} & & \rho_z^2 \end{pmatrix} \tag{2}$$

where $w_{\sigma 1}$ is a Gaussian convolutional kernel with standard deviation 3 voxels. In the last step, the eigenvalues and eigenvectors of $\mathrm{GST}(\rho)$ were extracted for each voxel and the eigenvector corresponding to the lowest eigenvalue was taken as the estimated *l*-direction. The result was a vector field $\boldsymbol{l}_{\mathrm{CT}}$ over the entire CT image.

A bounding boxing around the untwisted binary image was calculated to locate the initial surfaces of the sawn timber before planing. The calculation was performed by requiring that the outer slices of the bounding box contained a sufficiently large contiguous area of the untwisted binary image. From the outer slices, consecutive slices corresponding to the planing depths were extracted from the wide faces. For each slice, both the density values and the vector field of the estimated *l*-direction were extracted and exported for the subsequent synchronisation.

2.4 WOODEYE DATA PROCESSING

The WE data consisted of RGB intensity values and the in-plane fibre orientation angle α, which was defined as the shortest angle between the longitudinal scan direction (y) and the measured major axis of the ellipse formed by the laser point due to the tracheid effect. The data processing and the subsequent synchronisation was performed using code in MATLAB [15].

The data corresponded only to the scanned board surfaces and thus made a bounding box search unnecessary. Both the RGB and orientation data were available at points on non-uniform grids. To prepare the synchronisation, all WE data was therefore resampled by bicubic interpolation to the uniform grid of the corresponding slices from the untwisted CT image.

2.5 SYNCHRONISATION

Since some distortions existed in the WE data, e.g. due to the fact that the speed of the conveyor belt placed before the scanner was not perfectly aligned to the operational speed of the scanner, a mapping function needed to be

https://doi.org/10.52202/069179-0057

calculated to synchronise the WE data to the CT images. The synchronisation was based on the resampled WE RGB images of each face and the corresponding grayscale 2D slices obtained from the untwisted CT image.

The predrilled positioning holes served as an easily detectable reference in both representations and their centres were labelled manually in a user dialog in MATLAB by fitting circles, see Figure 4. The circle centres served as an input for calculating the mapping between the WE images to the CT faces. A projective 2D transformation matrix was estimated for performing the first part of the mapping, see Equation (3).

$$\begin{pmatrix} x' \\ y' \\ 1 \end{pmatrix} = \begin{pmatrix} r_1 & r_2 & t_1 \\ r_3 & r_4 & t_2 \\ p_1 & p_2 & 1 \end{pmatrix} \begin{pmatrix} x \\ y \\ 1 \end{pmatrix} \quad (3)$$

where x and y are the original coordinates of the wide face in the WE image, $x'$and y' are the coordinates after the projective transformation, and r_1 to r_4, t_1 and t_2, and p_1 and p_2 are the shear-rotational, translational, and projective coefficients of the transformation, respectively.

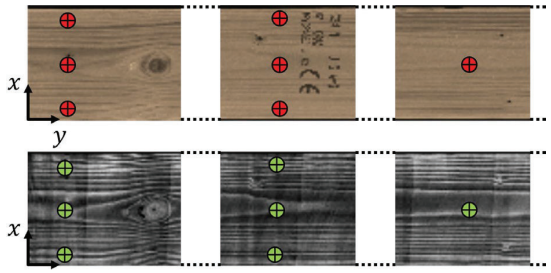

Figure 5: *Circle fitting in WE (top) and CT faces (bottom)*

Since a slight misalignment remained in the y-direction (lengthwise), cubic spline interpolation was used to map the y-coordinates of the transformed WE image (y') to a new set of y-coordinates (y'') that better match the CT image. The coefficients of the spline interpolation were calculated given the y-coordinates of the centres of the holes in the CT image along with the corresponding coordinates in the WE image after the projective transformation. The final transformation was composed of first applying the projective transformation and subsequently the spline interpolation.

The synchronisation needed to be performed separately for each surface of the sawn timber, and for each planing depth. Each calculated final transformation was applied to the corresponding WE data, i.e. both RGB and in-plane fibre orientation.

2.6 COMPARISON

The transformed WE data was compared to the untwisted CT image. The RGB images were converted to grayscale to visually compare it to the grayscale CT images. From the vector field $\boldsymbol{I}_{\mathrm{CT}}$, only the in-plane components were kept and compared to a vector field $\boldsymbol{I}_{\mathrm{WE}}$ which was derived from the WE orientations. Additionally, the absolute value of the in-plane angle $\mathrm{abs}(\alpha)$ of both representations was calculated and qualitatively compared in colour-coded plots.

3 RESULTS AND DISCUSSION

Below, the results of the synchronisation of a single piece of sawn timber are presented, for selected planing depths and primarily for the surface facing to the pith. The results differed little for the surfaces facing away from the pith.

3.1 SYNCHRONISATION MAPPING

Figure 6 shows the relative development of those parameters of the projective transformation matrix which were most different from zero, for increasing planing depth. The parameters associated with the perspective mapping differ before and after planing. The explanation for this is probably that when the holes were drilled with a handheld tool, the drill was not oriented perfectly perpendicular to the board face. Additionally, a human error factor was involved when manually locating the hole centres in the images.

Figure 7 shows the correction in y-direction from the spline interpolation after the projective transformation, for increasing planing depth. The characteristic of the correction is consistent for all planing depths, with decreasing amplitude at increasing planing depth, and with the profile being horizontally mirrored at mid-length of the board. The consistency of this transformation points to a systematic component in the distortion in the data.

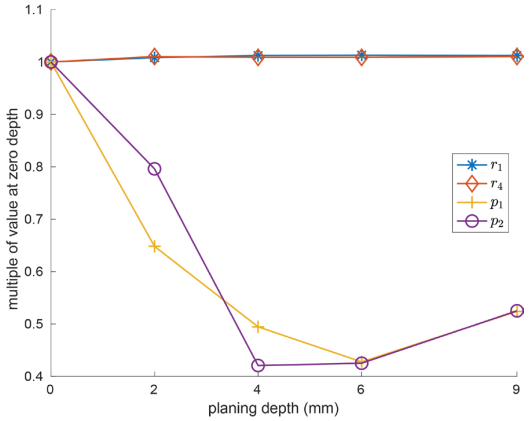

Figure 6*: Parameters of the projective transformation matrix as multiples of their respective values before planing*

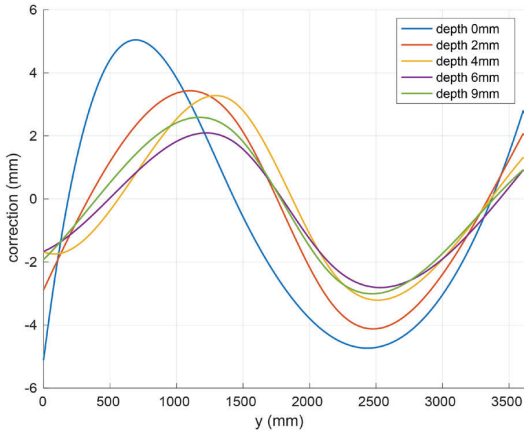

Figure 7*: Spline interpolation correction over the board length*

https://doi.org/10.52202/069179-0057

Figure 8 illustrates the alignment between WE and CT images for the surface of the board before planing, before and after the transformations at the positioning holes of one half of the board. After the projective transformation, a positioning error remained mostly at the holes towards the middle of the board. The error was decreased after the additional spline transformation.

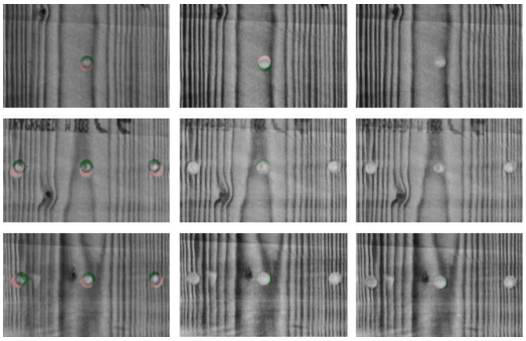

***Figure 8**: Hole alignment before transformation (left column), after projective transformation (middle), and after additional spline transformation (right), differences in red/green*

3.2 IN-PLANE FIBRE ORIENTATION

For a qualitative assessment, three regions along the board containing knots are reported, which comprised lengths of 160 mm in the proximity of the first, second and third row of positioning holes from one end of the board. Those regions will henceforth be referred to as region 1, 2 and 3.

Figures 9, 10 and 11 show the in-plane components of $\boldsymbol{l}_{WE}$ and $\boldsymbol{l}_{CT}$ plotted respectively on the transformed WE RGB image and the untwisted CT slice before planing of the surface facing the pith, and the corresponding angle, for regions 1, 2 and 3, respectively. Figures 12, 13 and 14 show the equivalent plots for a planing depth of 9 mm.

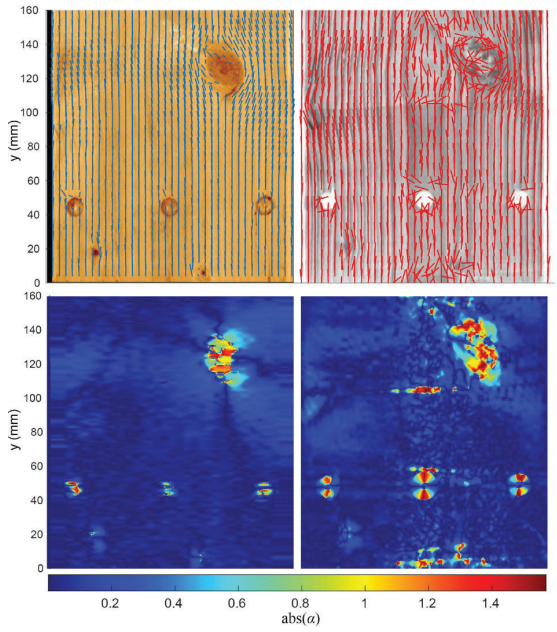

***Figure 9**: WE (left) and CT (right) in-plane vector fields (top) and orientation angle (bottom) for region 1 before planing*

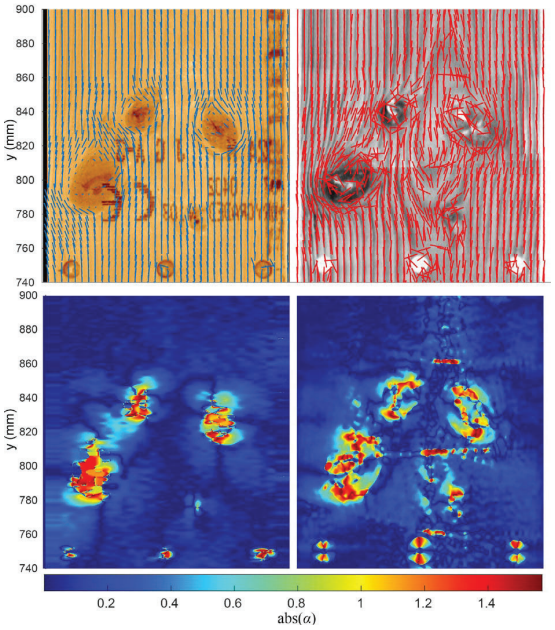

***Figure 10**: WE (left) and CT (right) in-plane vector fields (top) and orientation angle (bottom) for region 2 before planing*

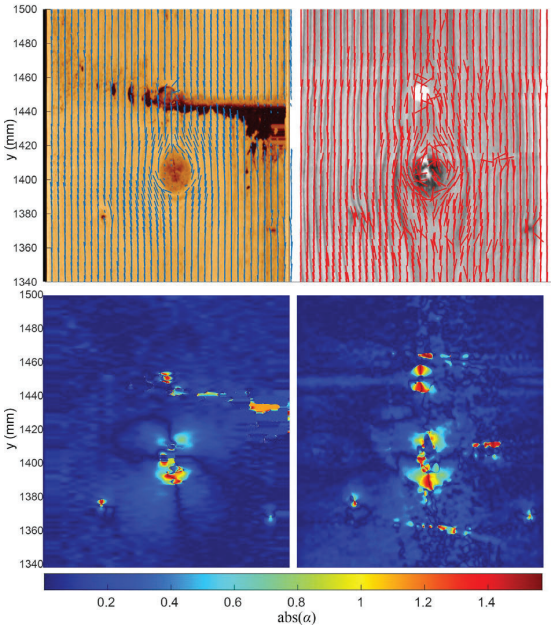

***Figure 11**: WE (left) and CT (right) in-plane vector fields (top) and orientation angle (bottom) for region 3 before planing*

Both, $\boldsymbol{l}_{WE}$ and $\boldsymbol{l}_{CT}$ reproduced a disturbed flow around the knots and a relatively laminar flow in regions without knots. Less variation existed in $\boldsymbol{l}_{WE}$ and the edges of the positioning holes were more clearly visible in $\boldsymbol{l}_{CT}$, due to the large density gradient between wood and air and the smaller pixel size in the CT image. However, $\boldsymbol{l}_{CT}$ was more sensitive to noise than $\boldsymbol{l}_{WE}$, in particular for the surface before planing, where the large density gradient between wood and air in the CT image affected the calculation of the GST. This effect is visible for regions 1 and 2 (Figures 9 and 10), where $\boldsymbol{l}_{CT}$ seems to follow the

https://doi.org/10.52202/069179-0057

apparent grain at the surface before planing, but it is less pronounced for the corresponding planed surfaces (Figures 12 and 13). Additionally, the plastic wrapping disturbed the calculation of $\boldsymbol{l}_{CT}$ in some regions where it was tightly packed. This is most clearly visible in Figure 10, where straight streaks across the surface in the CT image correspond to noise in α along equivalent streaks at the same locations. The field $\boldsymbol{l}_{CT}$ was generally more sensitive than $\boldsymbol{l}_{WE}$ to smaller knots and defects, due to its smaller original pixel size, resulting e.g. in deviations also around pitch pockets, see Figure 12.

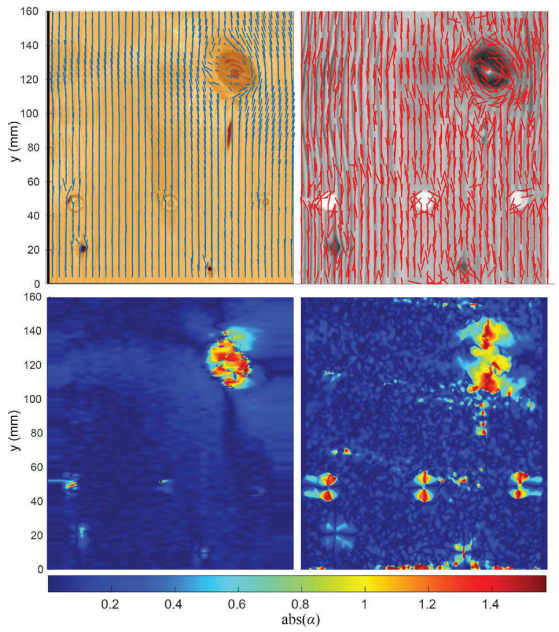

***Figure 12**: WE (left) and CT (right) in-plane vector fields (top) and orientation angle (bottom) for region 1 at a depth of 9 mm*

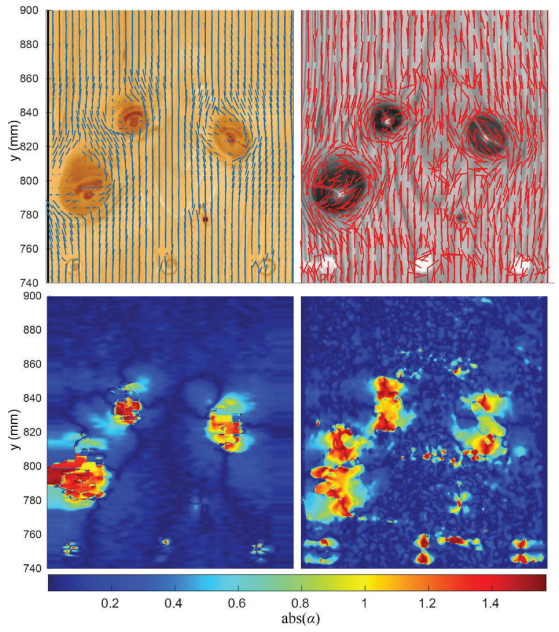

***Figure 13**: WE (left) and CT (right) in-plane vector fields (top) and orientation angle (bottom) for region 2 at a depth of 9 mm*

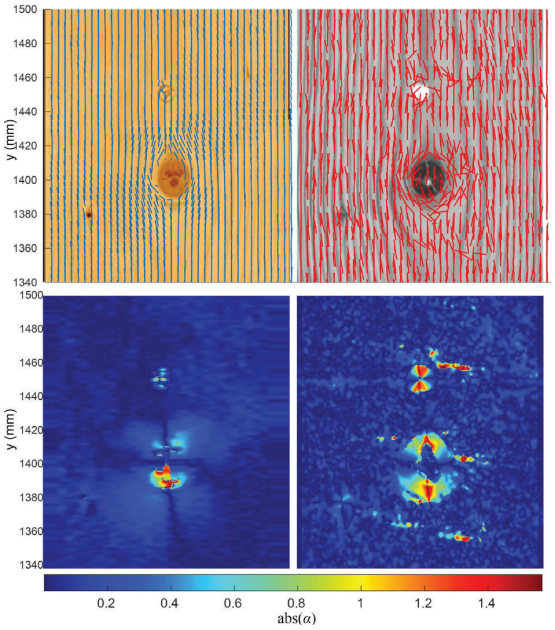

***Figure 14**: WE (left) and CT (right) in-plane vector fields (top) and orientation angle (bottom) for region 3 at a depth of 9 mm*

Figure 15 additionally shows the equivalent plot for region 2 before planing, but for the opposite side, i.e. the surface facing away from the pith. This surface included wane, which consequently affected the derived fibre orientations. For the CT image, vectors in the regions of wane can be removed easily by thresholding on density values. The field $\boldsymbol{l}_{CT}$ is notably affected by the apparent surface grain due to the surface effect described earlier.

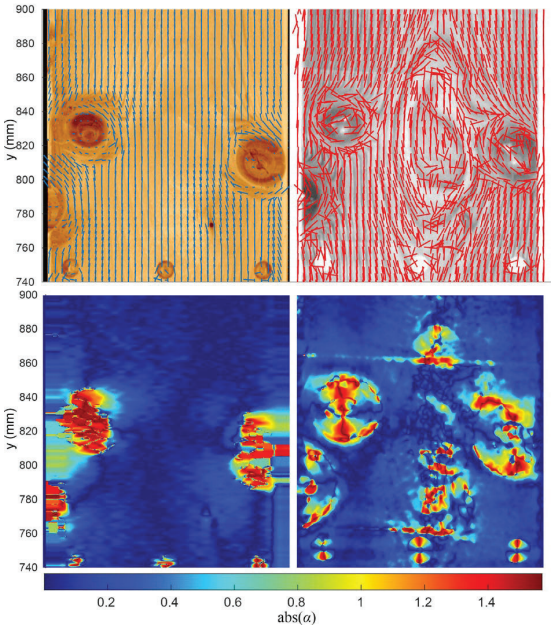

***Figure 15**: WE (left) and CT (right) in-plane vector fields (top) and orientation angle (bottom) for the surface facing away from the pith in region 2 before planing*

https://doi.org/10.52202/069179-0057

The field $\boldsymbol{l}_{CT}$ was strongly affected by the gradient out of plane in the shown image slices, e.g. inside knots where the *l*-direction followed the knot orientation, see Figure 16. For $\boldsymbol{l}_{WE}$, the out-of-plane component also followed the knot direction, but the in-plane component became generally less reliable due to small differences between the major and minor axes of the laser ellipse.

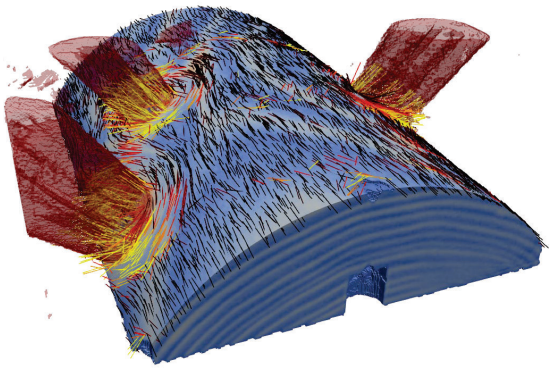

***Figure 16**: The field $\boldsymbol{l}_{CT}$ on a cylindrical cut around the pith in region 2 including segmented knot volumes*

4 CONCLUSION

In this study, optical scanning data of sawn timber was synchronised to corresponding CT images and the combined data set was used to compare and evaluate the fibre orientations derived from laser tracheid scanning and an image analysis-based method based on the density gradient structure. The results show that:

- a projective transformation in combination with a cubic spline interpolation for correction of the lengthwise position can synchronise the optical scanning data to a corresponding surface in the CT image,
- the in-plane fibre orientations calculated from the CT image gradients are qualitatively similar to the orientations derived from the optical data,
- the in-plane orientations from the CT image are more sensitive to noise and small defects, and they are less reliable on the original surface of the sawn timber.

The density gradient-based estimation of the fibre orientation should be further refined to reduce its sensitivity to noise. Further investigations are required on a larger number of samples to quantify the accuracy of this method, both in the vicinity of knots and in clearwood. To improve the accuracy of the synchronisation in future investigations, the location of the centres of the positioning holes should be automated, e.g. by ellipse fitting after an edge detection in the images, to minimise the effects of human error.

ACKNOWLEDGEMENT

The authors thank for the support of the Lennart & Alfhild Gabrielssons foundation, Swedish Wood (Svenskt Trä) and the CT-WOOD research programme in Skellefteå.

REFERENCES

[1] European Committee for Standardization (CEN): EN 408:2010+A1:2012, Timber structures - Structural timber and glued laminated timber - Determination of some physical and mechanical properties. 2012.

[2] Hanhijärvi A., Ranta-Maunus A. and Turk G.: Potential of strength grading of timber with combined measurement techniques. Report of the Combigrade-project - phase 2. VTT Publications 686, 2008.

[3] Olsson A. and Oscarsson J.: Strength grading on the basis of high resolution laser scanning and dynamic excitation: a full scale investigation of performance. *Eur. J. Wood Wood Prod.,* 75(1):17–31, 2017.

[4] Rais A. et al.: The use of the first industrial X-ray CT scanner increases the lumber recovery value: case study on visually strength-graded Douglas-fir timber. *Ann. For. Sci.*, 74(2):28, 2017.

[5] Longuetaud F. et al.: Automatic knot detection and measurements from X-ray CT images of wood: A review and validation of an improved algorithm on softwood samples. *Comput. Electron. Agric.*, 85:77–89, 2012.

[6] Hu M. et al.: Growth layer and fibre orientation around knots in Norway spruce: a laboratory investigation. *Wood Sci. Technol.*, 52: 7–27, 2018

[7] Hu M. et al.: Fibre directions at a branch-stem junction in Norway spruce: a microscale investigation using X-ray computed tomography. *Wood Sci. Technol.*, 56:147–169, 2022.

[8] Habite T., Abdeljaber O. and Olsson A.: Determination of pith location along Norway spruce timber boards using one dimensional convolutional neural networks trained on virtual timber boards. *Constr. Build. Mater.*, 329:127129, 2022.

[9] Lukacevic M. et al.: A 3D model for knots and related fiber deviations in sawn timber for prediction of mechanical properties of boards. *Mater. Des.*, 166:107617, 2019.

[10] Foley C.: Modeling the Effects of Knots in Structural Timber. PhD thesis, Lund University, 2003.

[11] Huber J. A. J. et al.: A method for generating finite element models of wood boards from X-ray computed tomography scans. *Comput. Struct.*, 260:106702, 2022.

[12] Bezanson, J. et al.: Julia: A fresh approach to numerical computing. SIAM review, 59(1): 65-98, 2017.

[13] Huber J. A. J.: Numerical Modelling of Timber Building Components to Prevent Disproportionate Collapse. PhD thesis, Luleå University of Technology, Skellefteå, 2021.

[14] Russ, J. C.: The Image Processing Handbook. 2nd ed. CRC Press, Boca Raton, FL, USA, 1995.

[15] MATLAB. version 9.13.0 (R2022b). Natick, Massachusetts: The MathWorks Inc., 2022.

https://doi.org/10.52202/069179-0057